

Fretting wear of bolted joint interfaces

Original

Fretting wear of bolted joint interfaces / Li, Dongwu; Botto, Daniele; Xu, Chao; Gola, Muzio. - In: WEAR. - ISSN 0043-1648. - ELETTRONICO. - 458-459:(2020), p. 203411. [10.1016/j.wear.2020.203411]

Availability:

This version is available at: 11583/2843468 since: 2020-08-31T12:10:35Z

Publisher:

Elsevier

Published

DOI:10.1016/j.wear.2020.203411

Terms of use:

This article is made available under terms and conditions as specified in the corresponding bibliographic description in the repository

Publisher copyright

Elsevier postprint/Author's Accepted Manuscript

© 2020. This manuscript version is made available under the CC-BY-NC-ND 4.0 license
<http://creativecommons.org/licenses/by-nc-nd/4.0/>. The final authenticated version is available online at:
<http://dx.doi.org/10.1016/j.wear.2020.203411>

(Article begins on next page)

Fretting wear of bolted joint interfaces

Dongwu Li¹, Daniele Botto², Chao Xu^{1,3*}, Muzio Gola²

¹*School of Astronautics, Northwestern Polytechnical University, Xi'an 710072, China*

²*Department of Mechanical and Aerospace Engineering, Politecnico di Torino, Turin 10129, Italy*

³*Qingdao R&D Institute, Northwestern Polytechnical University, Qingdao, 266200, China*

Abstract: Under vibration loading, fretting wear between bolted joint interfaces may change the dynamic characteristics of structures. Even the reliability of long-lasting assembly structures could be affected. This paper focuses on an experimental study on the fretting wear behavior of bolted joint interfaces under tangential loading. A recently developed fretting test apparatus was used to measure the hysteresis loops and the bolt preload at different fretting wear cycles. Changes of tangential contact stiffness and friction coefficient were estimated from the measured hysteresis loops. Experimental results showed a large change in bolt preload, contact stiffness, and friction coefficient due to fretting wear. The effect of surface roughness on fretting wear behavior of bolted joint interfaces was discussed. A modified Iwan model, comprehensive of wear effects, was proposed to simulate the hysteresis loops. Comparison between simulations and experimental results was performed to validate the proposed method. Results achieved in this research can provide the basis for the dynamic analysis of long-lasting joint structures in which wear plays a fundamental role in modifying the contact parameters.

Keywords: Fretting wear; bolted joint; hysteresis loop; contact parameters; Iwan model.

*Corresponding author: chao_xu@nwpu.edu.cn

Address: No. 127 Youyi West Road, Xi'an, Shaanxi 710072, China

22

1 Introduction

23 Bolted joints are widely used in mechanical assemblies. Connected parts are brought into contact
24 by bolt preload and transmit tangential loads by dry friction. Under oscillating loading, the contact
25 interfaces may undergo a relative motion with a small amplitude, which is referred to as fretting. There
26 are two main drawbacks associated with fretting: fretting fatigue and fretting wear. Roughly speaking,
27 fretting fatigue is associated with small relative displacements (micro-slip regime), whereas fretting
28 wear involves large relative displacements (gross slip regime). Fretting fatigue of bolted joints is
29 outside the scope of this article but it was studied in many papers [1-3]. The tangential friction force
30 plotted as a function of the relative displacement between the contact surfaces give the hysteresis loop.
31 This relationship exhibits a nonlinear behavior [4-6]. The area enclosed by the loop is the friction-
32 induced energy dissipation.

33 Increasing fretting wear cycles leads to material removal and change in interface topography.
34 Therefore, the contact behavior is modified because the contact stiffness and the friction-induced
35 damping varies with the fretting wear cycles. These changes significantly affect the dynamic
36 characteristics of joint structures [7-10]. At present, modeling fretting wear and its effects on the
37 dynamics of mechanical systems is becoming a major challenge in the field of the jointed structures.

38 A very good understanding of the physical phenomena associated with fretting wear helps in
39 modeling the behavior of joint interfaces. Yoon et al. [11] experimentally studied fretting wear in a
40 spherical contact subjected to constant normal load and measured the evolution of hysteresis loops.
41 The results revealed that the shape of hysteresis loops changed as a function of the number of fretting
42 cycles: the amplitude of relative displacement gradually decreased and the tangential force at the gross
43 slip stage increased. The dissipated energy per cycle increased in the first 500 cycles and then it
44 levelled off. Other similar results can be found in the literature [12, 13]. Fantetti et al. [8] measured
45 the hysteretic properties of a flat-on-flat contact pair and studied the effect of fretting wear on structural
46 dynamics. They replicated the evolution of hysteresis loops using a modified Bouc-Wen model
47 incorporating contact parameters evolution. Eriten et al. [14] investigated the effects of surface
48 roughness and lubrication on hysteresis loops at the early stage of the fretting of bolted joints. They

49 found the surface roughness influenced the shape of fretting loops and dissipated energy per cycle.
50 Lavella et al. [15-17] developed a flat-on-flat fretting test rig with high-temperature capability and
51 studied the effect of temperature on wear behavior. The results showed a significant dependence of the
52 hysteresis loops on the temperature.

53 Two contact parameters, namely the friction coefficient and the tangential contact stiffness, can
54 be used to replicate the hysteresis loop. Fretting wear can lead to significant changes in these
55 parameters. Almost all experimental studies found that both the friction coefficient and contact
56 stiffness rapidly increased during a running-in period [8, 11, 15, 18-23]. This trend was explained with
57 the interlocking between protrusions and depressions on the contact surfaces [19, 20]. As the wear
58 process continues, studies showed that the friction coefficient reached a peak, decreased and then
59 levelled off [20-23]. Other studies showed that the friction coefficient increased approaching a steady
60 state asymptote [8, 23]. Hintikka et al. [22] pointed out that the slight drop in the friction coefficient
61 was caused by wear debris. A reason for the stabilization in contact parameters was the balance
62 between generation and ejection of wear debris [8]. In addition, some works studied the effect of
63 surface roughness and high temperature on the evolution of contact parameters with increasing wear
64 [14, 15, 18, 21].

65 All the above-mentioned test cases had a constant normal load. This condition is different from
66 what we can find in bolted joints in which fretting wear could vary the preload.

67 The objective of this work is to investigate the effect of fretting wear on the behavior of bolted
68 joints. Fretting tests were performed to capture the evolution of hysteresis loops and of the associated
69 contact parameters. Tests were carried out using a recently developed fretting test rig. To evaluate the
70 effect of the bolt preload on the fretting behavior, the preload was monitored and recorded during each
71 test. The effects of surface roughness and sliding amplitude on fretting response was studied as well.
72 Moreover, a contact model was put forward to recreate hysteresis loops under different wear conditions.
73 A novel modified Iwan model, comprehensive of wear effects, was developed to simulate the hysteresis
74 loops.

75 The aim of these analysis was to promote a better understanding of fretting wear behavior of bolted
76 joint interfaces and to provide the modeling basis for the dynamic analysis of long-lasting joint

77 structures.

78 The paper is organized as follows. [Section 2](#) briefly describes the fretting test apparatus used in
79 this test campaign and details the wear test plan. [Section 3](#) shows the evolution of measured hysteresis
80 loops, bolt preloads and contact parameters with increasing wear cycles. The effects of surface
81 roughness on wear evolution are also discussed. [Section 4](#) models the evolution of contact parameters
82 and develops a modified Iwan model to replicate the evolution of hysteresis loops. [Section 5](#) discusses
83 the experimental findings and highlights the reliability of the numerical method.

84

2 Experimental Method

2.1 Description of the test apparatus

Experimental tests were conducted using the fretting test apparatus described in [24]. This rig was designed to study friction hysteresis behavior of bolted joint interfaces. Figure 1 shows the test apparatus and its main components. The joint is displaced by a piezoelectric actuator that moves one of the specimens, denoted as moving specimen, with an oscillating tangential displacement Δx . This displacement induces a tangential friction force at the contact surfaces. This force is measured with a dynamic load cell located at one end of the other specimen, denoted as fixed specimen. The relative displacement is measured by a laser vibrometer whose beam is bent with a prism. The bolt preload is measured with a force washer. Additional details and an accurate description of the working principle of the rig can be found in [24]. The measured contact friction force and the relative displacement give the well-known hysteresis loops. Tangential contact stiffness and friction coefficient can be extracted post-processing these loops.

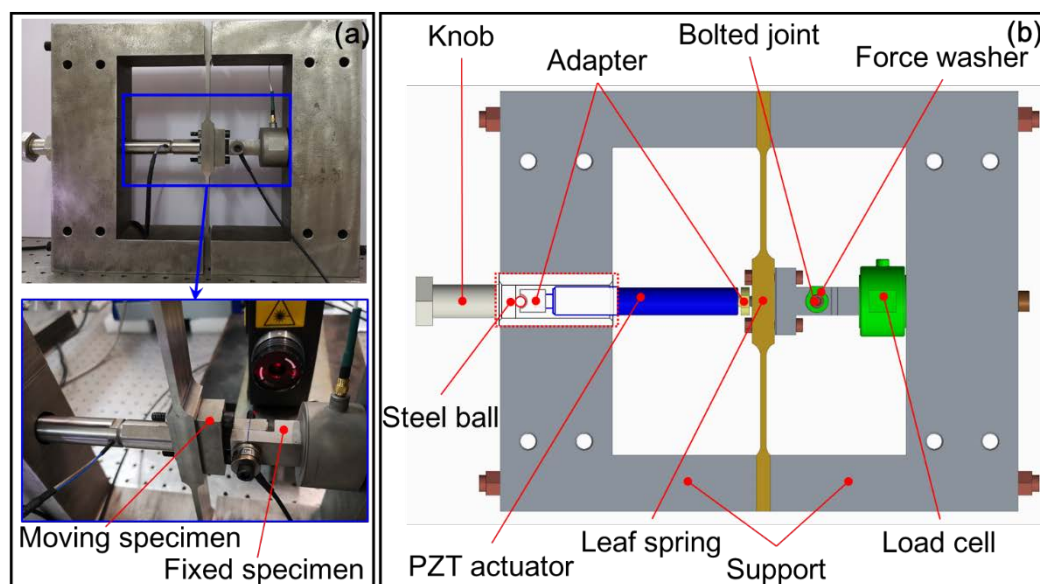


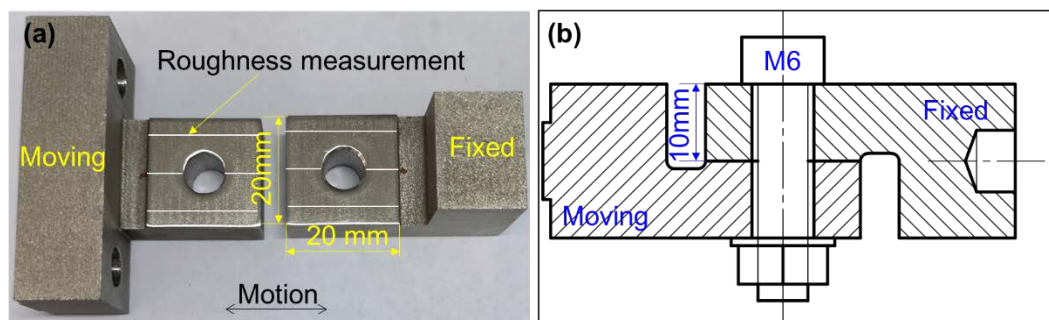
Fig. 1 (a) Photographs of the test apparatus, (b) Sketch of the test apparatus and main components.

The piezoelectric actuator is closed loop controlled using a built-in strain gauge sensor and a position servo controller. This control ensures the stability of excitation during fretting wear tests. The force-displacement data were continuously measured during the fretting test to monitor the evolution of hysteresis behavior. The tangential contact stiffness and the friction coefficient were extracted from

104 the hysteresis loops. The evolution of the bolt preload with the number of wear cycles was also
105 recorded as wear is one of the important reasons why the bolt preload is loosened [24-27].

106 2.2 Joint specimens

107 The bolted joint specimens are made of ASTM 304 stainless steel. The nominal contact region is
108 a 20 mm×20 mm square excluding the 7 mm diameter through hole. In these tests the bolt was an 8.8
109 M6. Figure 2 shows a photograph and a sketch of the bolted joint specimens.

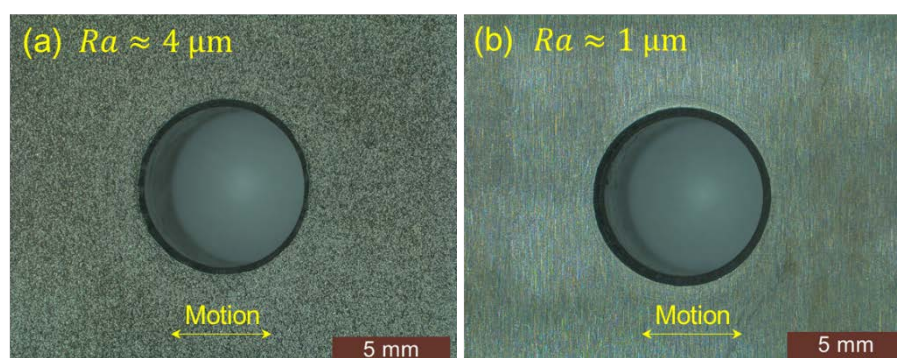


110

111 **Fig. 2** (a) Photograph of the joint specimens, (b) Sketch of the joint specimens

112 Joint specimens were manufactured by wire cutting, which leads to a large roughness of the
113 contact surface. The roughness was measured with a portable roughness profilometer. White lines in
114 Fig. 2(a) show the measurement paths selected along the sliding direction. The measurement length
115 was 4 and 2.4 mm on side and central lines, respectively. The average value of the measured roughness
116 was regarded as the roughness of the contact surface.

117 Specimens were divided into two groups, differing for surface roughness. The contact surfaces of
118 the first group were carefully hand-polished using two different grades of sandpaper (first 800 grit and
119 then 1200 grit), leading to a roughness R_a of about 1 μm . The contact surfaces of the second group of
120 specimens were not treated, and their roughness R_a was about 4 μm . Figure 3 shows photographs of
121 rough (second group) and smooth (first group) surfaces.



122

123 **Fig. 3** Photograph of the contact surfaces and corresponding surface roughness R_a , (a) rough surface:
 124 $R_a \approx 4 \mu\text{m}$, (b) smooth surface: $R_a \approx 1 \mu\text{m}$.

125 2.3 Wear test plan

126 Four fretting tests were conducted using different couples of joint specimens. The average
 127 roughness of the contact surface of each test specimen is shown in [Table 1](#). Two nominal tangential
 128 displacements, $\Delta x=50 \mu\text{m}$ and $40 \mu\text{m}$, were applied to the contact surfaces. The maximum allowable
 129 nominal displacement ($\Delta x=70 \mu\text{m}$) on the piezoelectric actuator was not applied as an excessive
 130 temperature due to long-lasting work could damage the piezoelectric.

131 **Table 1** Roughness R_a of the joint specimens for the tests 1/2/3/4, unit in μm

	Test 1	Test 2	Test 3	Test 4
Fixed specimen	4.34	0.78	4.27	0.81
Moving specimen	5.19	0.92	4.43	0.90

132

133 Tests were performed at a frequency of 25 Hz, that is far from resonance in the rig, as explained
 134 in [24]. The initial bolt preload was about 720 N for all tests, with a 5% scattering among different
 135 tests. This preload was chosen because it allowed to reach the selected excitation amplitudes and
 136 induce gross slip regime in the joint interface. Working in gross slip regime is a prerequisite for
 137 estimating the friction coefficients. Unlike the torque control method, this apparatus directly measures
 138 the preload using a force washer, so that the value of the preload can be controlled with great accuracy.
 139 The resulting nominal contact pressure was about 2 MPa. All tests were conducted at 25 °C and lasted
 140 12 hours (1.08 million wear cycles). [Table 2](#) summarizes the test specifications and operating
 141 conditions.

142 Data acquisition was performed with an in-house code written in LabVIEW 14.0. All forces and
 143 displacements were sampled at 5 kHz, and no filtering was applied. It was impossible to record 100%
 144 of the data because of the limited memory of the hard disk compared with the large amount of measured
 145 data. Therefore, the following acquisition strategy was used: for the first 20 minutes, 1-second data
 146 every 5 seconds was recorded; from 20 to 90 minutes, 1-second data every 40 seconds was recorded;
 147 from 90 to 720 minutes, 1-second data every 200 seconds was recorded.

148

Table 2 Summary of the wear test plan

	Test 1 / Test 2	Test 3 / Test 4
Material	Stainless steel	Stainless steel
Roughness, R_a	4 μm / 1 μm	4 μm / 1 μm
Excitation amplitude, Δx	50 μm	40 μm
Excitation frequency, f	25 Hz	25 Hz
Bolt preload, N_b	720 N	720 N
Running time	12 hours	12 hours
Temperature	25 $^{\circ}\text{C}$	25 $^{\circ}\text{C}$

149

150 Before and after each test, the specimens and the bolt were cleaned with alcohol in an ultrasonic
151 bath for 30 min to minimize the effects of particles and machine oil on test results. After cleaning,
152 microscopic images of contact surfaces were taken with a Leica S9D stereomicroscope.

153

3 Experimental results and discussion

154

Figure 4 illustrates an example of measured hysteresis loop. The area enclosed by the hysteresis

155

loop represents dissipated energy per cycle. The hysteresis loop can be characterized using two contact

156

parameters: tangential contact stiffness k_t and friction coefficient μ . The tangential contact stiffness

157

is determined by the slope of the force-displacement curve at the stick stage, $k_t = \Delta T / \Delta \delta$, see the

158

blue line in Fig. 4. The friction coefficient is usually defined as the ratio between the tangential and

159

the normal force during the gross slip regime. Results showed that the tangential force during the gross

160

slip regime was not constant, as pointed out by the red lines in Fig. 4. This behavior is due to the

161

residual stiffness that is caused by the bending of the bolt shank. A detailed analysis of the residual

162

stiffness was done in [24]. Therefore, the friction coefficient was determined in a different way. The

163

difference between the tangential force during the loading and unloading gross slip regime was $\Delta T =$

164

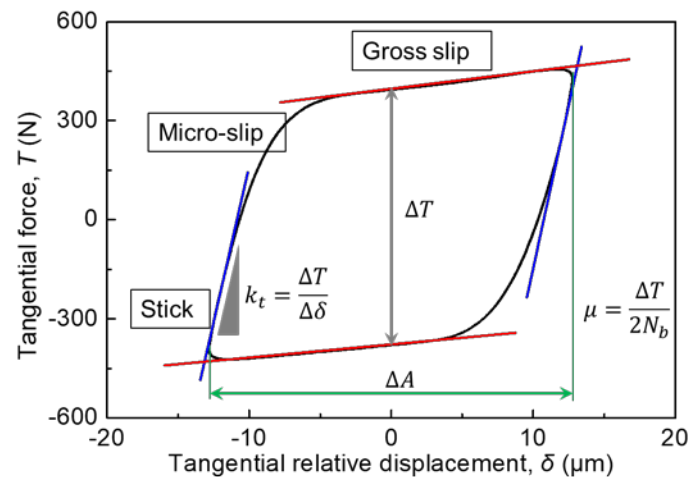
$T_{GS_load} - T_{GS_unload}$. This difference is visualized as the distance between the two red lines in Fig. 4.

165

In the difference ΔT , the contribution of the residual stiffness is cancelled. The friction coefficient can

166

be defined as the ratio between ΔT and twice the bolt preload, $\mu = \Delta T / 2N_b$.



167

Fig. 4. Typical hysteresis loop and schematic of the contact parameters extraction method.

168

169

3.1 Evolution of hysteresis loops

170

Figure 5 shows the evolution of the hysteresis loops during one million wear cycles. The shape of

171

hysteresis loops changed with increasing wear cycle. These changes were due to two main effects. The

172

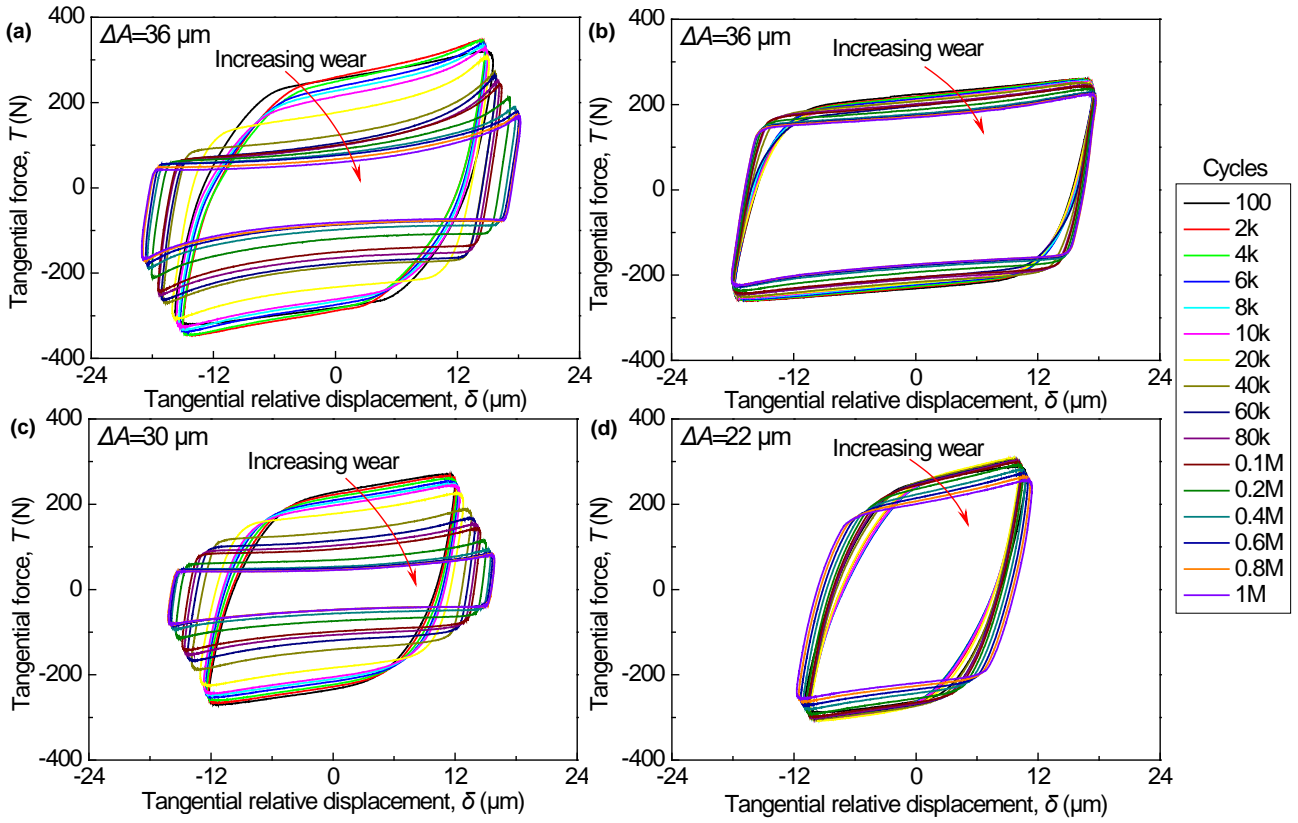
first effect was the modification of the contact surface and therefore of the friction coefficient and

173

contact stiffness. The second effect was the variation of the bolt preload. Variation in the hysteresis

174 loops was more evident in tests 1 and 3 (specimens with high roughness) than in test 2 and 4 (specimens
175 with low roughness). As a general trend, the tangential force at the gross slip stage gradually decreases
176 with increasing the wear cycles. For tests 1 and 2, the average sliding strokes, namely twice the
177 amplitude δ , ΔA were 36 μm ; in test 3 30 μm and in test 4 the average stroke was 22 μm . Rough
178 surfaces (tests 1 and 3) showed average sliding stroke more scattered than smooth surfaces (tests 2 and
179 4). [Figure 6](#) shows the normalized hysteresis loops, in which the tangential force was divided by the
180 bolt preload. The general trend was reversed with respect to the behavior shown in [Fig. 5](#) and the
181 normalized tangential force increases with the wear cycles. The normalized tangential force is related
182 to friction coefficient. It will be discussed in section 3.3.

183 An additional phenomenon can be observed in the tests. The force-displacement curve at the end
184 of the gross slip stage exhibits a bulge – stiffness hardening – after about 0.1 million wear cycles. The
185 higher the amplitude of the relative displacement, the more evident was the stiffness hardening. This
186 phenomenon was observed in several wear experiments [15, 20, 23, 28, 29], but the physical reason
187 was not fully understood yet. There are two possible explanations: (i) interaction among wear scars
188 that are not present on the new contact surfaces and (ii) the bolt pinning effect, that is, the bolt shank
189 getting in contact with the through hole.

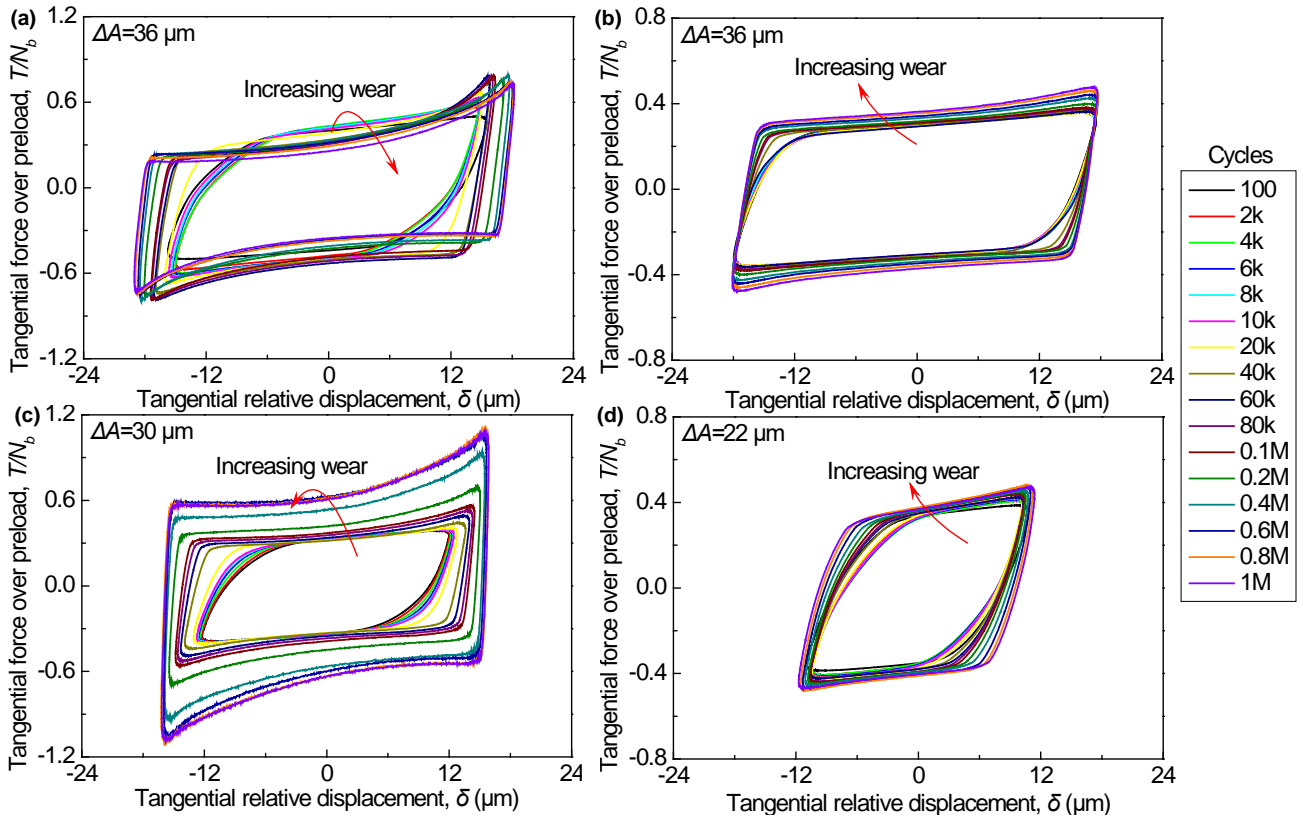


190

191 **Fig. 5.** Evolution of hysteresis loops with increasing wear, (a) Test 1: $\Delta x = 50 \mu\text{m}$, $R_a \approx 4 \mu\text{m}$, (b)

192 Test 2: $\Delta x = 50 \mu\text{m}$, $R_a \approx 1 \mu\text{m}$, (c) Test 3: $\Delta x = 40 \mu\text{m}$, $R_a \approx 4 \mu\text{m}$, (d) Test 4: $\Delta x =$

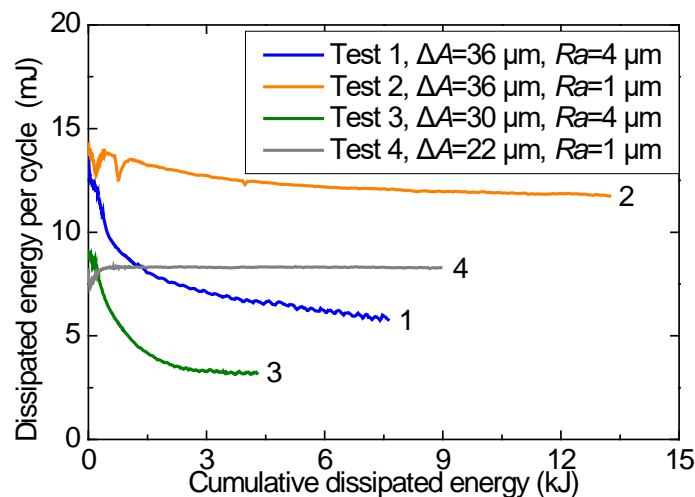
193 $40 \mu\text{m}$, $R_a \approx 1 \mu\text{m}$.



194

195 **Fig. 6.** Tangential force versus bolt preload for different tests, (a) Test 1: $\Delta x = 50 \mu\text{m}$, $R_a \approx 4 \mu\text{m}$, (b)
 196 Test 2: $\Delta x = 50 \mu\text{m}$, $R_a \approx 1 \mu\text{m}$, (c) Test 3: $\Delta x = 40 \mu\text{m}$, $R_a \approx 4 \mu\text{m}$, (d) Test 4: $\Delta x =$
 197 $40 \mu\text{m}$, $R_a \approx 1 \mu\text{m}$.

198 **Figure 7** plots the evolution of the dissipated energy per cycle E_c as a function of the cumulative
 199 dissipated energy E . In tests 1 and 3, the dissipated energy per cycle decreased and then gradually
 200 stabilized. The dissipated energy in the final state is 42% and 25% of the initial value, respectively. In
 201 tests 2 and 4, the dissipated energy showed a short period of oscillation and then gradually reached a
 202 steady state. And the change in dissipated energy E_c was much lower. In test 2, the dissipated energy
 203 E_c in the final state was 84% of the initial value. In test 4, the dissipated energy E_c almost remained
 204 unchangeable after the initial oscillation. The dissipated energy per cycle in tests 2 and 4 (low
 205 roughness) was significantly larger than in tests 1 and 3 (high roughness), except for the first thousand
 206 cycles.



207

208

Fig. 7. Dissipated energy per cycle for the different tests.

209

3.2 Evolution of bolt preloads

210

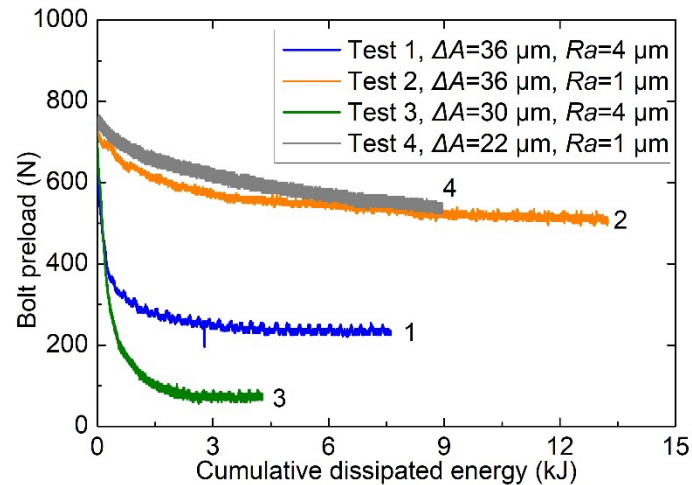
211

212

213

214

Wear tests are usually performed with a constant normal load [8, 15, 19, 29, 30]. Differently from
 standard test, in this work the normal load was not constant because the bolt preload varied with wear
 cycles. **Figure 8** illustrates the variation of bolt preloads with the cumulative dissipated energy. In all
 tests, the bolt preloads showed a trend with a steep descent then it approached to an asymptotic steady-
 state value.



215

216

Fig. 8. Bolt preloads for the different tests.

217

218

219

220

221

222

223

224

225

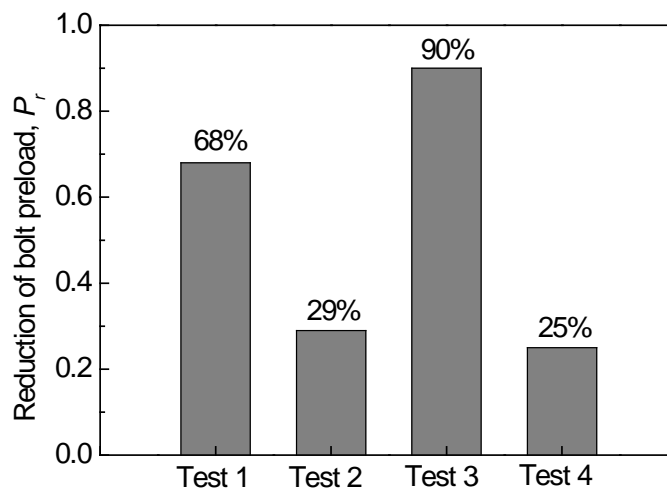
226

227

228

229

Tests performed in this work showed that in tests 1 and 3 the reduction in bolt preload was more than that in tests 2 and 4. Figure 9 depicts the percentage reduction in bolt preload, $P_r = (N_{b-initial} - N_{b-end}) / N_{b-initial}$, where $N_{b-initial}$ represents the initial value of the bolt preload, and N_{b-end} its final value. The preload reduction was more pronounced for the contact surfaces with higher roughness than for lower roughness. In test 3 the reduction even reached 90% of the initial value while in tests 2 and 4 the preload reduction was less than 30%. The decrease in bolt preload under transversal vibration was widely investigated in the literature. A reasonable explanation of preload loosening is that the peaks of micro-protrusions of rough surfaces are cut and flattened during the wear process. The interference fit between the contact surfaces is reduced, which in turn results in preload decreasing. Experimental results pointed out that rough surfaces experienced greater bolt preload drop off than smooth surfaces. Recent investigations [25] revealed that the main cause of preload loosening at the early stage was the stress release and the redistribution of threaded teeth. In [25] the effect of roughness was not investigated.



230

231 **Fig. 9.** Reduction in bolt preload with respect to the initial value in the four tests, $N_{b-initial}$ represents
 232 the initial value of the bolt preload, and N_{b-end} its final value.

233 **3.3 Evolution of contact parameters**

234 It is known that the contact stiffness and the friction coefficient are notably affected by the wear
 235 of contact surfaces [8, 15, 23]. The contact parameters were computed according to the procedure
 236 described in Section 3 and summarized in Fig. 4.

237 **3.3.1 Tangential contact stiffness**

238 Figure 10(a) plots the contact stiffness as a function of the cumulative dissipated energy E . Results
 239 showed a large variation of the contact stiffness. Contact stiffness in test 1 was higher than in test 3
 240 even if they showed a similar behavior: contact stiffness first experienced a rapid and significant
 241 increase, reaching a peak at about 13 kJ of dissipated energy, then they decreased. Figure 10(b) presents
 242 the contact stiffness as a function of the bolt preload and shows that the contact stiffness increased
 243 even if the bolt preload decreases. Several experimental evidences indicate that higher normal load
 244 gives higher contact stiffness. On the other hand, theoretical result using the Mindlin solution [31]
 245 reveals that the contact stiffness is proportional to the radius of the contact area and does not depend
 246 on the normal load, as shown in Eq.(1)

$$k_t = \frac{8Ga}{2 - \nu} \quad (1)$$

247 where G , a and ν denote shear modulus, radius of the contact area and Poisson's ratio, respectively.

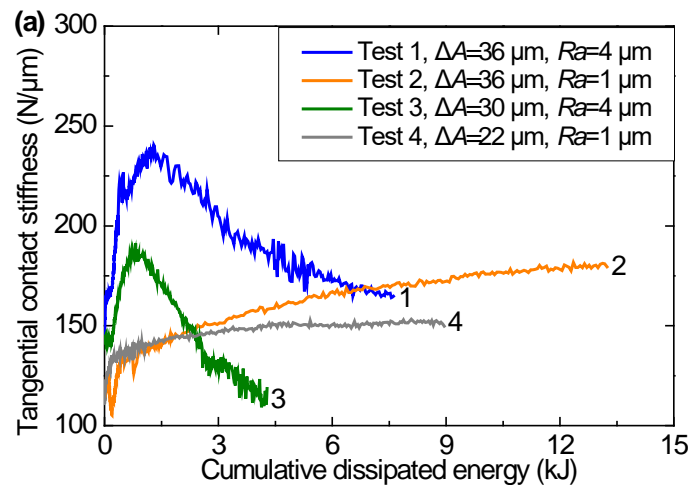
248 Therefore, the relationship between the normal load and the contact stiffness appears to be related to

249 the change in the contact area: increasing the normal load increases the contact area and therefore the

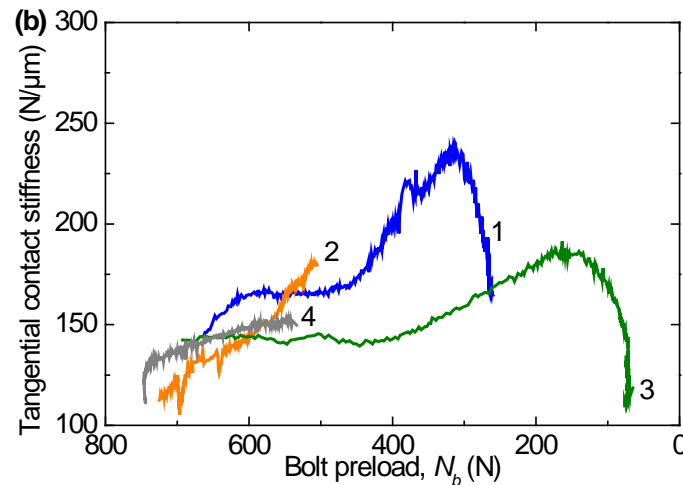
250 contact stiffness. In our tests the normal load was variable and diminished with the wear cycles,
251 therefore, the contact stiffness was expected to decrease. Due of the wear process, the contact area
252 increased and therefore the contact stiffness also increased.

253 The contact stiffness can also be related to the height of the asperity at the interfaces [8, 19]. The
254 initial contact stiffness of the rough surfaces (test 1 and test 3) was significantly greater than that of
255 the smooth surfaces (test 2 and test 4). Therefore, the increase in contact stiffness may be mainly
256 caused by the increased interaction between wear scars. This interaction increases the resistance to the
257 relative motion between the contact surfaces at the stick stage. When the bolt preload drops to a certain
258 level, the preload dominates the change in contact stiffness. This resulted in reduced contact stiffness
259 after the peak.

260 In tests 2 and 4, the contact stiffness also increased at the early stage of fretting wear, then it
261 gradually stabilized. The same trend was observed in the experiments reported in [8, 23] where the
262 normal load was constant during the wear tests and the contact surface roughness was about $1\ \mu\text{m}$. In
263 these experiments, the reduction in bolt preload was negligible, so that modification of the contact
264 surfaces was the main reason for the variation of the contact stiffness.



265

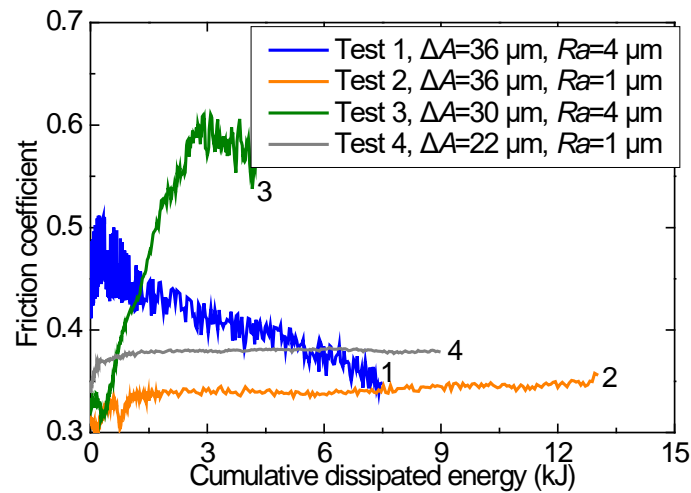


266

267 **Fig. 10.** Tangential contact stiffness depending on (a) cumulative dissipated energy, and (b) bolt
 268 preload.

269 **3.3.2 Friction coefficient**

270 The trend of the friction coefficient for the four tests is shown in Figure 11. Tests 1 and 3 showed
 271 a similar trend. In test 1, the friction coefficient increased, it reached the peak and then decreased with
 272 evident fluctuations. In test 3, the friction coefficient peaked at about 3 kJ, the peak value (0.6) was
 273 about two times the initial value (0.3), then it decreased slowly with evident oscillations. These
 274 oscillations are due to the production of debris, that increases the friction coefficient, and are then
 275 discharged reducing the friction. Friction coefficients in tests 2 and 4 showed a similar trend that is
 276 different from the behavior observed in tests 1 and 3. The friction coefficients increased at the early
 277 stages and then gradually leveled off. This behavior was observed also in [8, 15, 22, 23, 32]. As
 278 explained in [33], in the early stage the coefficient of friction increases due to a rapid increase in the
 279 number of wear particles entrapped between the sliding surfaces. As the wear process go on the
 280 frictional force decreases, due to the decrease in asperity deformation and ploughing. The steady state
 281 condition is reached when the generation of new wear particles balance the particles leaving the
 282 interface and the surface becomes mirror smooth as a result of the wear process. Tests point out the
 283 role of the roughness. Surface with higher roughness shows a larger variation of the friction coefficient
 284 than surface with lower roughness. Higher asperities are easier to cut by shear loads and larger debris
 285 is generated.



286

287

Fig. 11. Evolution of friction coefficients with cumulative energy dissipated.

288

3.4 Worn surfaces

289

290

291

292

293

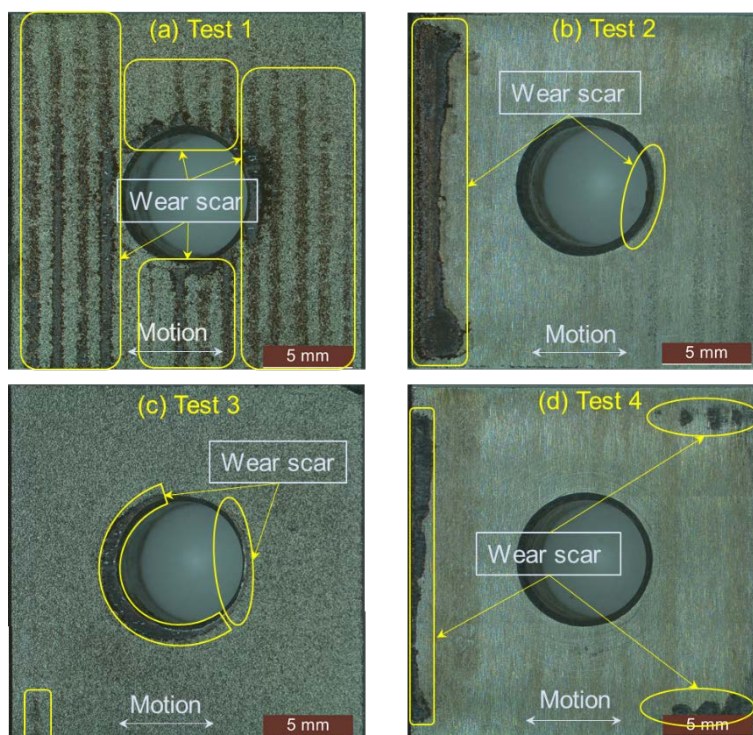
294

295

296

297

Microscopic images of contact surfaces were obtained by a stereomicroscope. Figure 12 shows the photographs of contact surfaces after fretting wear tests. In these images wear scars are surrounded by yellow lines. Wear scars are distributed in different way for different tests. In test 1, the wear scars are some vertical stripes that are evenly distributed along the direction of movement. These stripes coincide with traces of wire cutting. Most likely, the manufacturing process left the contact surface with pronounced waviness. In test 3, the wear scars are mainly found around the through hole, probably because of the protrusion of the hole edges due to the drilling process. In tests 2 and 4, wear scars are mainly distributed near the left border of the contact surfaces, with only a small part on the right. This is probably caused by the hand-polished process.



298

299 **Fig. 12.** Contact surface images after fretting wear tests, (a) Test 1: $\Delta x = 50 \mu\text{m}$, $Ra \approx 4 \mu\text{m}$, (b) Test

300 2: $\Delta x = 50 \mu\text{m}$, $Ra \approx 1 \mu\text{m}$, (c) Test 3: $\Delta x = 40 \mu\text{m}$, $Ra \approx 4 \mu\text{m}$, (d) Test 4: $\Delta x = 40 \mu\text{m}$, $Ra \approx$

301 $1 \mu\text{m}$.

302

4 Modeling wear-induced hysteresis loops evolution

In the past decades, several contact models have been developed to replicate friction hysteresis loops, such as Iwan model [34-36], Bouc-Wen model [37] and LuGre model [38]. In this work, based on the framework of the Iwan model, we introduce parameters that depend on the wear cycles.

4.1 Wear-dependent parameters

The Iwan model [36] can be defined by using 3 parameters: tangential contact stiffness k_t , friction coefficient μ and normal preload N_b . The original Iwan model is not able to simulate the residual stiffness phenomenon, therefore a new parameter, namely the residual stiffness k_r , was introduced. In this work, the parameters in the Iwan model are formulated as functions of the cumulative dissipated energy E .

To simulate the evolution of parameters with wear (wear-dependent parameters), a set of exponential basis functions, reported in Table 3, was selected. The coefficients of these basis functions were obtained by fitting the experimental results. The same functions were used for tests 2 and 4. The subscript '0', N_{b0} , k_{t0} and μ_0 , denotes the initial values of contact parameters. The exponents of the basis functions, c and d were the same for different parameters and were obtained through a best fit procedure with the least square method. Results of the best fit procedure showed that these exponents are the same for similar contact conditions, for example tests 2 and 4. Results of the best fit procedure are shown in Table A1 (see Appendix A). Coefficients a_i ($i=1, 2, 3$) of the basis functions are the ratio between the final value and the initial value of the contact parameter. Coefficients b_i ($i=1, 2$) are the multiplier of the basis functions and with range $[0, 1]$. Details about these coefficients can be found in Appendix A. The residual stiffness was considered independent of wear cycles as it is related to the bending stiffness of the bolt shank that is not affected by the change in bolt preloads [24]. Results in Fig. 13(d) support the above assumption.

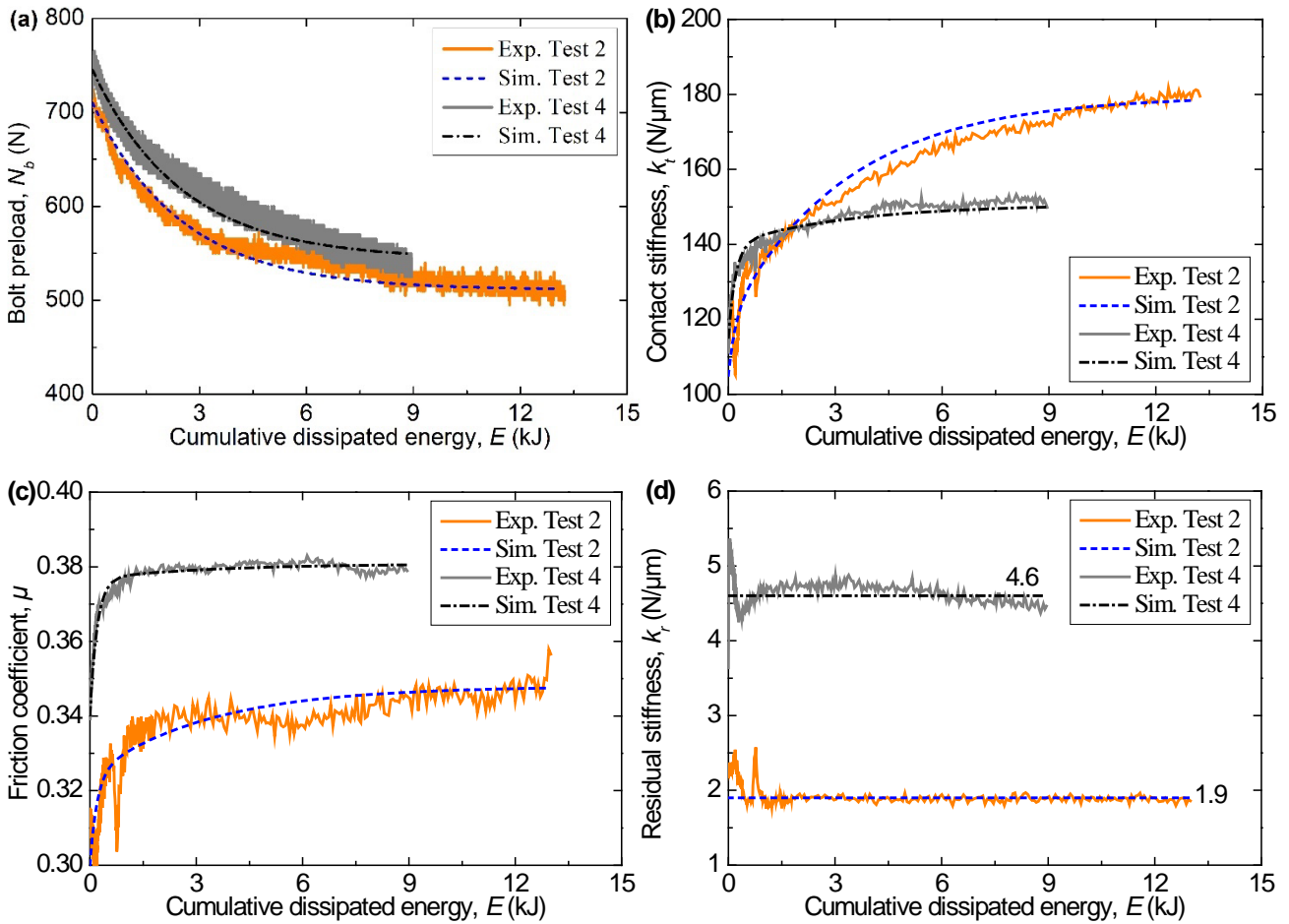
Figure 13 shows the wear-dependent parameters of tests 2 and 4 as a function of the energy E and compares the analytical parameters, as defined in Table 3, with the measured parameters.

Table 3 Functions of wear-dependent contact parameters

Variables	Functions
Bolt preload	$N_b(E) = N_{b0}[a_1 + (1 - a_1)e^{cE}]$

Contact stiffness	$k_t(E) = k_{t0}\{a_2 + (1 - a_2)[b_1 e^{cE} + (1 - b_1)e^{dE}]\}$
Friction coefficient	$\mu(E) = \mu_0\{a_3 + (1 - a_3)[b_2 e^{cE} + (1 - b_2)e^{dE}]\}$

329



330

331

332 **Fig. 13.** Wear-dependent parameters for tests 2 and 4: (a) Bolt preload; (b) tangential contact stiffness;
 333 (c) friction coefficient; (d) residual stiffness.

334 **4.2 Iwan model with wear-dependent parameters**

335 The Iwan model is composed of infinite number of Jinkins elements in parallel. These elements
 336 have the same contact stiffness and different critical sliding force. The sum of the critical sliding force
 337 on each element is equal to Coulomb friction force μN_b and it is distributed to each element with a
 338 uniform density function. The Iwan model can reproduce stick, micro-slip and gross slip behavior of
 339 contact surfaces under tangential vibrations. A detailed description of the Iwan model and its recent
 340 improvement for using in modeling joint can be found in [34-36].

341 The original Iwan model was modified to consider the effect of the residual stiffness. For a
 342 monotonic loading case, the force-displacement relationship of the modified Iwan model is written as

$$T_m(\delta) = \begin{cases} (k_t + k_r)\delta - \frac{(k_t\delta)^2}{4\mu N_b}, & \delta < \frac{2\mu N_b}{k_t + k_r} \\ \mu N_b + k_r\delta, & \delta > \frac{2\mu N_b}{k_t + k_r} \end{cases} \quad (2)$$

343 where T_m is the tangential force and δ the tangential relative displacement. For a cyclic loading case,
 344 the force-displacement relationship can be obtained by substituting Eq. (2) into Eq. (3),

$$T(\delta) = \begin{cases} -T_m(\delta_m) + 2T_m\left(\frac{\delta_m + \delta}{2}\right), & \dot{\delta} > 0 \\ T_m(\delta_m) - 2T_m\left(\frac{\delta_m - \delta}{2}\right), & \dot{\delta} < 0 \end{cases} \quad (3)$$

345 where T is the tangential force and δ_m the amplitude of tangential relative displacements.

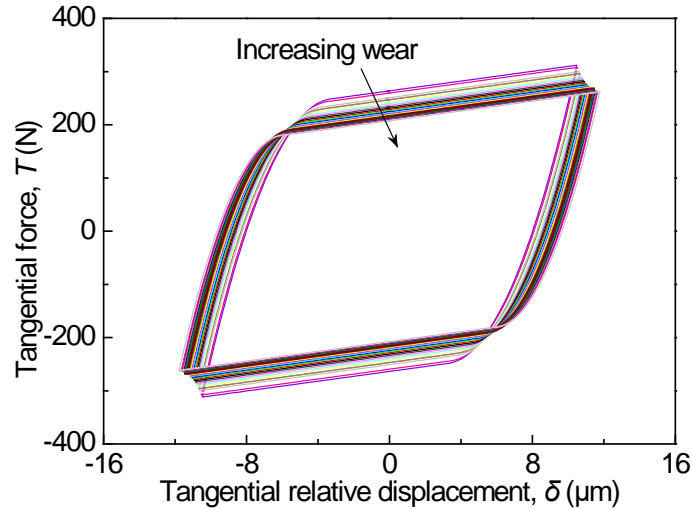
346 The wear-dependent parameters are included in the modified Iwan model to simulate the effect of
 347 wear on the friction behavior. The resulting force-displacement relationship for monotonic loading
 348 case is

$$T_m(\delta, E) = \begin{cases} [k_t(E) + k_r(E)]\delta - \frac{[k_t(E)\delta]^2}{4\mu(E)N_b(E)}, & \delta < \frac{2(E)N_b(E)}{k_t(E) + k_r(E)} \\ \mu(E)N_b(E) + k_r(E)\delta, & \delta > \frac{2(E)N_b(E)}{k_t(E) + k_r(E)} \end{cases} \quad (4)$$

349 Substituting Eq. (4) into Eq. (3) yields the force-displacement relationship for the cyclic loading
 350 case. In Eq. (4) there are two independent variables, namely δ and E , that have different time scales.
 351 The cumulative dissipated energy is defined over one period of vibration and it is a step function in
 352 the time function. In the process of calculating hysteresis loops the step size of the cumulative
 353 dissipated energy E is the period of vibration.

354 After each vibration period, the cumulative dissipated energy is recalculated. Then the contact
 355 parameters are updated for the next vibration period. Performing this operation cyclically results in the
 356 hysteresis loops involving wear evolution. Figure 14 depicts the evolution of the hysteresis loops with
 357 increasing wear simulated by the proposed method.

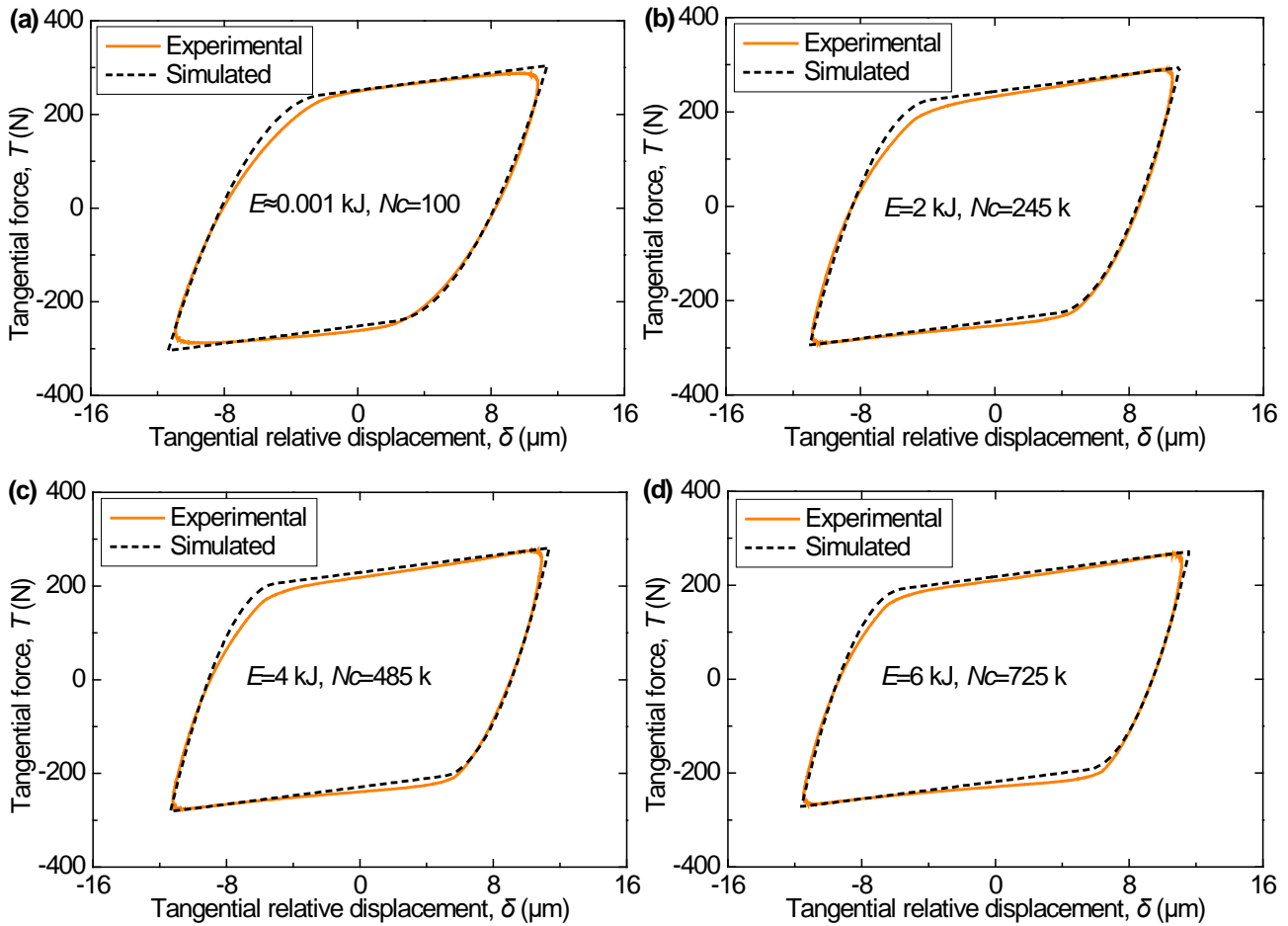
358 To assess the effectiveness of the proposed method, a set of simulated results were compared with
 359 the experimental counterparts. Figure. 15 shows the results of the comparison that are in good
 360 agreement with the measured hysteresis loops.



361

362

Fig. 14. Evolution of simulated hysteresis loops with increasing wear for test 4.



363

364

Fig. 15. Comparison between simulated and experimental hysteresis loops in test 4: (a) $E \approx 1$ J, $N_c=100$; (b) $E = 2$ kJ, $N_c=245$ k; (c) $E = 4$ kJ, $N_c=485$ k; (d) $E = 6$ kJ, $N_c=725$ k. N_c is the number of wear cycle.

367

368

5 Conclusions

369 Prior works have documented how fretting wear influenced the contact parameters and the
370 dynamic behavior of structures. These early studies did not consider the interaction between fretting
371 wear and bolt preload. This work investigated the fretting wear behavior of bolted joint interfaces.
372 Tests were performed with an apparatus specifically designed to measure the friction hysteresis
373 behavior of bolted joint. The tangential contact force and the relative displacements were measured at
374 different stages of wear. Contact parameters, tangential stiffness and friction coefficient, were extracted
375 from the hysteresis loops and their evolution monitored with wear cycles. Bolt preloads were also
376 recorded continuously during the tests.

377 Experimental results showed that the surface roughness significantly influenced the evolution of
378 the contact parameters. For the same sliding amplitude, the higher the surface roughness, the more
379 drastic the change in the shape of the hysteresis loop. Hysteresis loops on rough surfaces showed a
380 residual stiffness that gradually decreases with wear cycles. Moreover, the tangential force decreased
381 with the wear cycles and the gross slip regime became predominant. The preload decreased with wear
382 cycles as well and since the tangential force is related to the bolt preload the two results are consistent.
383 Preload on rough surface at the end of the test was 10% of the initial preload. Smooth surfaces showed
384 a reduction in the preload that was much less than that of the rough surfaces. Higher asperities are
385 easily deformed or cut, and these processes led to reduction of the interference fit between the
386 connected part, which in turn resulted in reduction of the bolt preload.

387 The contact stiffness is mainly driven by the true contact area that in turn increases with the normal
388 load. Since the contact stiffness increased with decreasing the preload, this is a clear evidence that the
389 increase in the contact area due to the wear process overcame the decrease in contact area due to the
390 decrease in the preload. Contact stiffness for rough surfaces showed a peak when the preload becomes
391 very low. Preload on smooth surfaces did not reach such low values of preload and a comparison is
392 not possible.

393 The friction coefficient of rough and smooth surfaces showed a remarkable different behavior.
394 The friction coefficient of smooth surfaces increased and then levelled off. On the other hand, the

395 friction coefficient of rough surface increased up to a peak, decreased and then levelled off. For the
396 rough surfaces, the wear process is more prone to produce wear particles. Wear particles entrapped in
397 the contact surfaces are the main reason for the increase in friction coefficient in the early state of wear.
398 When debris generated by the wear process balance the debris ejected outside the contact, the friction
399 coefficient stabilized towards a steady-state value.

400 In this study, a contact model was developed to simulate the fretting wear behavior of bolted joint
401 interfaces. This method reconstructs the evolution of contact parameters using a set of wear-dependent
402 coefficients. Dependence on wear was formulated in terms of cumulative dissipated energy. These
403 coefficients were introduced in the well-known Iwan model to replicate the evolution of hysteresis
404 loops with wear. The simulated and measured hysteresis loops were in good agreement and prove the
405 reliability of the proposed numerical method. It should be noted that the proposed wear-dependent
406 coefficients can also be combined with other contact models. The developed method can be used to
407 simulate the dynamics of bolted joint structures in which fretting wear process heavily alters the
408 contact conditions.

409

410

Acknowledgments

411 The authors wish to acknowledge and thank the China Science Challenge for funding their research
412 project (TZ2018007). Dongwu Li would also like to show his gratitude to China Scholarship Council
413 (CSC) for supporting him as a visiting Ph.D. to AERMEC lab of Politecnico di Torino within the
414 project EXTHENdED.

415

Appendix A: Coefficients of wear functions

416

417 **Table A1** lists the coefficients of wear functions developed in section 4.1. The coefficient a_i ($i =$
 418 $1, 2, 3$) is defined as the ratio of the final value of contact parameters to the initial value. The
 419 coefficients c and d are the exponents of the basis function. Tests 2 and 4 have the same coefficients
 420 a_i, c and d . The coefficient b_i ($i = 1, 2$) is the multiplier of the basis function and is in the range $[0,$
 421 $1]$. This coefficient is different for different tests. Even so, a general value $b_i = 0.5$ can be selected
 422 for different tests to some extents.

423

Table A1 Coefficients of wear functions

Variables	Tests 2 and 4 (the same coefficients)	Test 2	Test 4
Bolt preload	$a_1 = N_{be}/N_{b0}, c = -0.3$		
Contact stiffness	$a_2 = k_{te}/k_{t0}, c = -0.3, d = -5$	$b_1 = 0.3$	$b_1 = 0.8$
Friction coefficient	$a_3 = \mu_e/\mu_0, c = -0.3, d = -5$	$b_2 = 0.2$	$b_2 = 0.5$

424

425 **References**

- 426 [1] A. Ferjaoui, T. Yue, M.A. Wahab, R. Hojjati-Talemi, Prediction of fretting fatigue crack initiation
427 in double lap bolted joint using Continuum Damage Mechanics, *International Journal of Fatigue*, 73
428 (2015) 66-76. <https://doi.org/10.1016/j.ijfatigue.2014.11.012>.
- 429 [2] J. Juoksukangas, A. Lehtovaara, A. Mantyla, Experimental and numerical investigation of fretting
430 fatigue behavior in bolted joints, *Tribology International*, 103 (2016) 440-448. [https://doi.org/10.1016](https://doi.org/10.1016/j.triboint.2016.07.021)
431 [/j.triboint.2016.07.021](https://doi.org/10.1016/j.triboint.2016.07.021).
- 432 [3] C. Jimenez-Pena, R.H. Talemi, B. Rossi, D. Debruyne, Investigations on the fretting fatigue failure
433 mechanism of bolted joints in high strength steel subjected to different levels of pre-tension, *Tribology*
434 *International*, 108 (2017) 128-140. <https://doi.org/10.1016/j.triboint.2016.11.014>.
- 435 [4] L. Gaul, R. Nitsche, The Role of Friction in Mechanical Joints, *Applied Mechanics Reviews*, 54
436 (2001) 93-106. <https://doi.org/10.1115/1.3097294>.
- 437 [5] M.R.W. Brake, et al. *The Mechanics of Jointed Structures: Recent Research and Open Challenges*
438 *for Developing Predictive Models for Structural Dynamics*. Springer, 2017. [https://doi.org/10.1007/](https://doi.org/10.1007/978-3-319-56818-8)
439 [978-3-319-56818-8](https://doi.org/10.1007/978-3-319-56818-8).
- 440 [6] D. Botto, M. Lavella, A numerical method to solve the normal and tangential contact problem of
441 elastic bodies, *Wear*, 330-331 (2015) 629-635. <https://doi.org/10.1016/j.wear.2015.02.046>.
- 442 [7] E. Lemoine, D. Nélias, F. Thouverez, C. Vincent, Influence of fretting wear on bladed disks
443 dynamic analysis, *Tribology International*, 145 (2020) 106148. [https://doi.org/10.1016/j.triboint.2019.](https://doi.org/10.1016/j.triboint.2019.106148)
444 [106148](https://doi.org/10.1016/j.triboint.2019.106148).
- 445 [8] A. Fantetti, L.R. Tamatam, M. Volvert, I. Lawal, L. Liu, L. Salles, M.R.W. Brake, C.W.
446 Schwingshackl, D. Nowell, The impact of fretting wear on structural dynamics: Experiment and
447 Simulation, *Tribology International*, 138 (2019) 111-124. [https://doi.org/10.1016/j.triboint.2019.](https://doi.org/10.1016/j.triboint.2019.05.023)
448 [05.023](https://doi.org/10.1016/j.triboint.2019.05.023).
- 449 [9] L. Salles, L. Blanc, F. Thouverez, A.M. Gousskov, Dynamic analysis of fretting-wear in friction
450 contact interfaces, *International Journal of Solids and Structures*, 48 (2011) 1513-1524.
451 <https://doi.org/10.1016/j.ijsolstr.2011.01.035>.
- 452 [10] J. Armand, L. Pesaresi, L. Salles, C.W. Schwingshackl, A Multiscale Approach for Nonlinear
453 Dynamic Response Predictions With Fretting Wear, *Journal of Engineering for Gas Turbines and*
454 *Power*, 139 (2017) 022505. <https://doi.org/10.1115/1.4034344>.
- 455 [11] Y. Yoon, I. Etsion, F.E. Talke, The evolution of fretting wear in a micro-spherical contact, *Wear*,
456 270 (2011) 567-575. <https://doi.org/10.1016/j.wear.2011.01.013>.
- 457 [12] M.R. Hirsch, R.W. Neu, A simple model for friction evolution infretting, *Wear*, 301 (2013) 517-
458 523. <https://doi.org/10.1016/j.wear.2013.01.036>.
- 459 [13] T. Liskiewicz, S. Fouvry, Development of a friction energy capacity approach to predict the
460 surface coating endurance under complex oscillating sliding conditions, *Tribology International*, 38
461 (2005) 69-79. <https://doi.org/10.1016/j.triboint.2004.06.002>.
- 462 [14] M. Eriten, A.A. Polycarpou, L.A. Bergman, Effects of surface roughness and lubrication on the
463 early stages of fretting of mechanical lap joints, *Wear*, 271 (2011) 2928-2939.
464 <https://doi.org/10.1016/j.wear.2011.06.011>.
- 465 [15] M. Lavella, D. Botto, M.M. Gola, Design of a high-precision, flat-on-flat fretting test apparatus

- 466 with high temperature capability, *Wear*, 302 (2013) 1073-1081.
467 <https://doi.org/10.1016/j.wear.2013.01.066>.
- 468 [16] Botto D, Campagna A, Lavella M, Gola, MM. Experimental and numerical investigation of
469 fretting wear at high temperature for aeronautical alloys. *Proceedings of the ASME Turbo Expo. 2010*;
470 6: 1353-1362. <https://doi.org/10.1115/GT2010-23356>.
- 471 [17] M. Lavella, D. Botto, Fretting Fatigue Analysis of Additively Manufactured Blade Root Made of
472 Intermetallic Ti-48Al-2Cr-2Nb Alloy at High Temperature, *Materials*, 11 (2018). <https://doi.org/10.3390/ma11071052>.
- 473
474 [18] M. Lavella, D. Botto, Fretting wear characterization by point contact of nickel superalloy
475 interfaces, *Wear*, 271 (2011) 1543-1551. <https://doi.org/10.1016/j.wear.2011.01.064>.
- 476 [19] M.E. Kartal, D.M. Mulvihill, D. Nowell, D.A. Hills, Measurements of pressure and area
477 dependent tangential contact stiffness between rough surfaces using digital image correlation,
478 *Tribology International*, 44 (2011) 1188-1198. <https://doi.org/10.1016/j.triboint.2011.05.025>.
- 479 [20] D.M. Mulvihill, M.E. Kartal, A.V. Olver, D. Nowell, D.A. Hills, Investigation of non-Coulomb
480 friction behaviour in reciprocating sliding, *Wear*, 271 (2011) 802-816. <https://doi.org/10.1016/j.wear.2011.03.014>.
- 481
482 [21] K.J. Kubiak, T.G. Mathia, S. Fouvry, Interface roughness effect on friction map under fretting
483 contact conditions, *Tribology International*, 43 (2010) 1500-1507. <https://doi.org/10.1016/j.triboint.2010.02.010>.
- 484
485 [22] J. Hintikka, A. Lehtovaara, A. Mäntylä, Fretting-induced friction and wear in large flat-on-flat
486 contact with quenched and tempered steel, *Tribology International*, 92 (2015) 191-202. <https://doi.org/10.1016/j.triboint.2015.06.008>.
- 487
488 [23] C.W. Schwingshackl, E.P. Petrov, D.J. Ewins, Measured and estimated friction interface
489 parameters in a nonlinear dynamic analysis, *Mechanical Systems and Signal Processing*, 28 (2012)
490 574-584. <https://doi.org/10.1016/j.ymssp.2011.10.005>.
- 491 [24] Li D., Xu C., Botto D., et. al. A novel test apparatus for measuring friction hysteresis of bolted
492 joints, *Tribology International*, 2020, Under review.
- 493 [25] H. Gong, J. Liu, X. Ding, Study on the mechanism of preload decrease of bolted joints subjected
494 to transversal vibration loading, *Proceedings of the Institution of Mechanical Engineers, Part B: Journal of Engineering Manufacture*, 233 (2019) 2320-2329. <https://doi.org/10.1177/0954405419838675>.
- 495
496
497 [26] Y. Jiang, M. Zhang, C.-H. Lee, A Study of Early Stage Self-Loosening of Bolted Joints, *Journal of Mechanical Design*, 125 (2003) 518-526. <https://doi.org/10.1115/1.1586936>.
- 498
499 [27] R.I. Zadoks, X. Yu, An investigation of the self-loosening behavior of bolts under transverse
500 vibration, *Journal of Sound and Vibration*, 208 (1997) 189-209. <https://doi.org/10.1006/jsvi.1997.1173>.
- 501 [28] D. Botto, M. Lavella, High temperature tribological study of cobalt-based coatings reinforced
502 with different percentages of alumina, *Wear*, 318 (2014) 89-97. <https://doi.org/10.1016/j.wear.2014.06.024>.
- 503
504 [29] S. Fouvry, P. Duó, P. Perruchaut, A quantitative approach of Ti-6Al-4V fretting damage: friction,
505 wear and crack nucleation, *Wear*, 257 (2004) 916-929. <https://doi.org/10.1016/j.wear.2004.05.011>.
- 506 [30] M. Gonzalez-Valadez, A. Baltazar, R.S. Dwyer-Joyce, Study of interfacial stiffness ratio of a
507 rough surface in contact using a spring model, *Wear*, 268 (2010) 373-379. <https://doi.org/10.1016/j.wear.2010.03.014>.

508 [wear.2009.08.022](https://doi.org/10.1016/j.wear.2009.08.022).

509 [31] R.D. Mindlin, W.P. Mason, T.F. Osmer, et al. Effects of an oscillating tangential force on the
510 contact surfaces of elastic spheres. *J. Appl. Mech.* 18 (1951) 331-331. [https://doi.org/ 10.1007/978-1-
511 4613-8865-4_32](https://doi.org/10.1007/978-1-4613-8865-4_32).

512 [32] M.E. Kartal, D.M. Mulvihill, D. Nowell, D.A. Hills, Determination of the Frictional Properties of
513 Titanium and Nickel Alloys Using the Digital Image Correlation Method, *Experimental Mechanics*,
514 51 (2011) 359-371. <https://doi.org/10.1007/s11340-010-9366-y>.

515 [33] N.P. Suh, H.C. Sin, The genesis of friction. *Wear*, 69(1) (1981) 91-114. [https://doi.org/10.1016/
516 0043-1648\(81\)90315-X](https://doi.org/10.1016/0043-1648(81)90315-X).

517 [34] W.D. Iwan, A Distributed-Element Model for Hysteresis and Its Steady-State Dynamic Response,
518 *Journal of Applied Mechanics*, 33 (1966) 893-900. <https://doi.org/10.1115/1.3625199>.

519 [35] D. Li, D. Botto, C. Xu, T. Liu, M. Gola, A micro-slip friction modeling approach and its
520 application in underplatform damper kinematics, *International Journal of Mechanical Sciences*, 161-
521 162 (2019) 105029. <https://doi.org/10.1016/j.ijmecsci.2019.105029>.

522 [36] D. Li, C. Xu, T. Liu, M.M. Gola, L. Wen, A modified IWAN model for micro-slip in the context
523 of dampers for turbine blade dynamics, *Mechanical Systems and Signal Processing*, 121 (2019) 14-30.
524 <https://doi.org/10.1016/j.ymsp.2018.11.002>.

525 [37] F. Ikhouane, J. Rodellar, On the Hysteretic Bouc–Wen Model, *Nonlinear Dynamics*, 42 (2005)
526 63-78. <https://doi.org/10.1007/s11071-005-0069-3>.

527 [38] K. Johansson, C. Canudas-de-Wit, Revisiting the LuGre friction model, *IEEE Control Systems
528 Magazine*, 28 (2008) 101-114. <https://doi.org/10.1109/MCS.2008.929425>.

529